JOURNAL OF GEOPHYSICAL RESEARCH, VOL. 114, D13303, doi:10.1029/2009JD011785, 2009

Processes regulating short-lived species in the tropical tropopause layer

A. Gettelman,[1] P. H. Lauritzen,[2] M. Park,[1] and J. E. Kay[2,3]

Received 22 January 2009; revised 29 March 2009; accepted 30 April 2009; published 8 July 2009.

[1] A one-dimensional model of vertical transport in the tropical tropopause layer (TTL) is developed. The model uses vertical advection, a convective source, and a chemical sink to simulate the profiles of very short lived substances in the TTL. The model simulates evanescent profiles of short-lived hydrocarbon species observed by satellite and is also used to simulate short-lived bromine species. Tracers with chemical lifetimes of 25 days or longer have significant concentrations in the stratosphere, and vertical advection is critical. Convection is important up to its peak altitude, nearly 19 km. Convection dominates the distribution of species with lifetimes less than 25 days. The annual cycle of species with lifetimes longer than 25 days is governed primarily by the variations of vertical velocity, not convection. This is particularly true for carbon monoxide, where a seasonal cycle in the lower stratosphere of the right phase is produced without variations in tropospheric emissions. An analysis of critical short-lived bromine species (CH_2Br_2 and $CHBr_3$) indicates that substantial amounts of these tracers may get advected into the lower stratosphere as source gases at 18 km, and are estimated to contribute 2.8 pptv (1.1–4.1) to stratospheric bromine.

Citation: Gettelman, A., P. H. Lauritzen, M. Park, and J. E. Kay (2009), Processes regulating short-lived species in the tropical tropopause layer, *J. Geophys. Res.*, *114*, D13303, doi:10.1029/2009JD011785.

1. Introduction

[2] Transport in the region around the tropical tropopause, the tropical tropopause layer (TTL), is important for setting the chemical boundary conditions of the stratosphere. This is particularly true for species with lifetimes $<\sim$2 months, whose chemical or removal lifetime is comparable to or shorter than the transit time through the TTL, estimated at $\sim$60 days [*Fueglistaler et al.*, 2004]. One important example are bromine compounds, which can turn bromine into active forms that can efficiently deplete ozone in the stratosphere. Currently there are large uncertainties of the reactive bromine in the lower stratosphere [*Salawitch et al.*, 2005; *World Meteorological Organization*, 2007]. Uncertainty is driven by sources, as well as how very short lived substances (VSLS: defined here as lifetimes <6 months) enter the stratosphere through the TTL. There is also uncertainty in how dehydration and wet removal occurs [*Sinnhuber and Folkins*, 2006].

[3] Transport in the TTL occurs through rapid vertical motion in deep convection and slow vertical transport outside of clouds. The TTL transit time for each pathway may be very different, and the impact on trace species may be very different [*Fueglistaler et al.*, 2009]. Transit may vary in space and time, with some regions such as the boreal summer Asian Monsoon contributing disproportionally [*Gettelman et al.*, 2004b]. Washout of chemical species may also be important [*Sinnhuber and Folkins*, 2006].

[4] In this work we develop a model of the TTL that simulates the effect of key processes on chemical constituents in order to better understand the balance of processes responsible for TTL transport. The model is similar to those developed by *Read et al.* [2004] to examine water vapor dehydration in the TTL and *Sinnhuber and Folkins* [2006] to explore bromoform ($CHBr_3$) in the stratosphere.

[5] The model is an idealized model of mean tropical transport that simulates tracers with various lifetimes, and compares the resulting profiles to satellite observations. We will focus on the effect of convective transport, large-scale vertical motions and chemical production or loss in the region. Our goal is to determine the range of tracer lifetimes that result in significant stratospheric injection, and for key bromine containing species, quantify how much bromine they may carry into the stratosphere. Section 2 contains a description of the methodology, section 3 describes the model, section 4 contains results, and conclusions are in section 5.

2. Methodology and Observations

2.1. Observations for Comparison

[6] Observations from the Atmospheric Chemistry Experiment (ACE) Fourier Transform Spectrometer (FTS) provide information on short-lived species in the TTL.

[1]Atmospheric Chemistry Division, National Center for Atmospheric Research, Boulder, Colorado, USA.
[2]Climate and Global Dynamics Division, National Center for Atmospheric Research, Boulder, Colorado, USA.
[3]Also at Department of Atmospheric Science, Colorado State University, Fort Collins, Colorado, USA.

0148-0227/09/2009JD011785$09.00

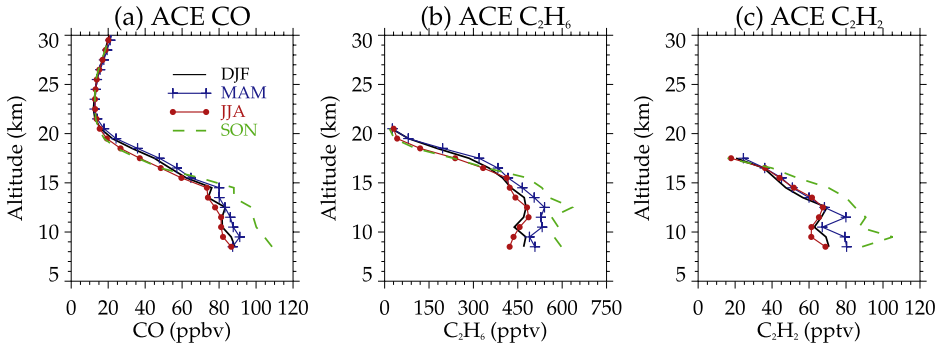

Figure 1. ACE tropical (20°S–20°N) average mixing ratios for 2004–2006 by season for (a) CO, (b) C_2H_6, and (c) C_2H_2.

ACE-FTS is a limb-viewing Fourier Transform Spectrometer [*Bernath et al.*, 2005]. ACE is in an orbit designed to maximize observations at high latitudes, but limited information is available for the tropics. Retrievals of species with different lifetimes from ACE surrounding the Asian Monsoon for the data used here representing 2004–2006 were presented by *Park et al.* [2008].

[7] Figure 1 shows ACE profiles of three tracers with very different lifetimes. Data represent 130–220 profiles in each season between 20°S–20°N latitude from 2004–2006. Carbon monoxide (CO) has a lifetime of ~60 days. Ethane (C_2H_6) has a lifetime of ~45 days and acetylene (C_2H_2) has a lifetime of ~15 days. Tracers fall off rapidly with height above 12–15 km, higher for species with longer lifetimes. Seasonally, there are higher tropospheric concentrations of all three tracers in September–November (SON) in the troposphere, and higher concentrations of CO and C_2H_6 in the TTL (16–20 km). Table 1 shows the annual average fraction of tracer remaining at various altitudes from Figure 1. The shorter-lived species have a lower fraction of their tropospheric mixing ratio remaining at any altitude, and this decreases rapidly above the tropopause.

[8] ACE observations of these hydrocarbons represent a range of lifetimes. We also run the model with tracers more representative of short-lived bromine and iodine containing species that might affect stratospheric ozone: Dibromomethane (CH_2Br_2) with a lifetime of 120 days, bromoform ($CHBr_3$) with a lifetime of 26 days and methyl iodide (CH_3I) with a lifetime of 6 days [*World Meteorological Organization*, 2007]. We do not have satellite observations of these species in the TTL for comparison with simulations.

2.2. Why a One-Dimensional Model?

[9] Three-dimensional (3-D) motions are critical for understanding the complex motions and interactions between convective and large-scale processes in the TTL. There have been many studies analyzing processes in the TTL using 3-D trajectory-based models [*Gettelman et al.*, 2002a; *Fueglistaler and Haynes*, 2005] or complex coupled chemistry-climate models [*Gettelman and Birner*, 2007]. However, there still is utility in using simple column models to try to understand processes, such as those explored by *Sherwood and Dessler* [2001]. Simple models allow complex processes to be reduced to a few simple relationships, and allow results to be directly related to individual terms or processes. They also allow rapid sensitivity testing of the parameter space of simulated processes. Results can be designed to compare to observations at similar scales. It is in this spirit that we develop and present a one-dimensional (1-D) vertical transport model for short-lived species in the TTL.

[10] The model is similar to previous 1-D and 2-D models of the TTL. *Sinnhuber and Folkins* [2006] used the TTL convective detrainment model of *Folkins and Martin* [2005] to investigate how bromoform is transported in the TTL, and found significant transport of bromine into the stratosphere occurred. Transport was dependent on the assumed washout rate for bromine. *Read et al.* [2004, 2008] used a version of the model originally developed by *Holton and Gettelman* [2001] and *Gettelman et al.* [2002a] to look at transport of tracers such as water vapor and carbon monoxide seasonally in the TTL. Here we develop a 1-D model to explore a variety of short-lived species and look at the transport times into the stratosphere.

3. Model Description

[11] This section describes the basic formulation of the 1-D transport model and the inputs used to drive the model.

3.1. Transport

[12] The model is constructed as a one-dimensional transport model, with a basic tendency equation for each tracer,

$$\frac{\partial [X_i]}{\partial t} = \frac{\partial [X_i]_{adv}}{\partial t} + \frac{\partial [X_i]_{conv}}{\partial t} + \frac{\partial [X_i]_{loss}}{\partial t} + \frac{\partial [X_i]_{mix}}{\partial t}, \qquad (1)$$

where $[X_i]$ is the mixing ratio of tracer i, and the tendencies correspond to vertical advection (*adv*), a convective source (*conv*), parameterized chemical loss (*loss*) and mixing (*mix*).

Table 1. Percent of Surface Source Remaining at Given Altitudes for Tracers With Different Lifetimes (December–February) Based on ACE-FTS Observations

Tracer	Lifetime, Days	Percent Remaining		
		16 km/100 hPa	18 km/79 hPa	20 km/58 hPa
CO	60	75	50	25
C_2H_6	45	67	42	12
C_2H_2	15	57	29	4

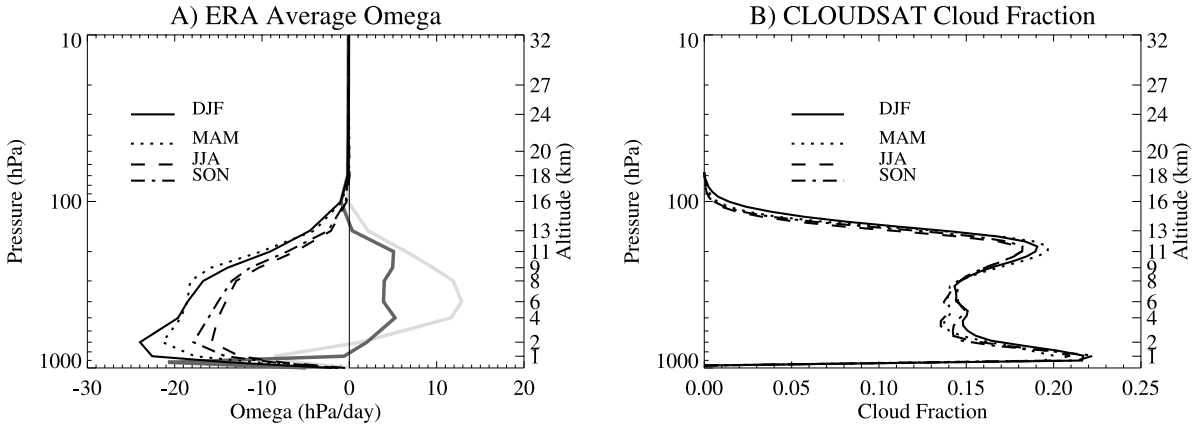

Figure 2. Tropical averaged (20°S–20°N) seasonal profiles used as input for the simulations. (a) Omega (pressure vertical velocity) from ECMWF analysis. (b) CloudSat cloud fraction. Light gray line in Figure 2a is December–February (DJF) omega calculated only for regions where the outgoing longwave radiation (OLR) is greater than 240 W m^{-2} as described in the text. Dark gray line in Figure 2a is DJF omega sorted by regions where the CloudSat cloud fraction is less than 0.15.

[13] The advective tendency for tracer i is given by the flux-form conservation equation

$$\frac{\partial [X_i]_{adv}}{\partial t} = -\nabla \cdot (\vec{v}\,[X_i]) - \frac{\partial}{\partial p}(\omega\,[X_i]), \tag{2}$$

where $\vec{v}$ is the horizontal velocity vector, p the pressure and ω the vertical velocity in pressure coordinates. Making the assumption that the horizontal distribution of tracer i is uniform, equation (2) can be written as

$$\frac{\partial [X_i]_{adv}}{\partial t} = -[X_i]\,\nabla \cdot \vec{v} - \frac{\partial}{\partial p}(\omega\,[X_i]). \tag{3}$$

[14] The horizontal divergence ($\nabla \cdot \vec{v}$) is prescribed as well as the vertical velocity in pressure coordinates (ω). We solve the vertical part of equation (3) using the first-order finite-volume scheme of *Godunov* [1959], which is mass-conservative and positive definite. Omitting the horizontal term, a finite-volume discretization of equation (3) simply states that the rate of change of tracer mass at a given column level with pressure thickness Δp, $\partial([X_i]\Delta p)/\partial t$, is given by the flux of tracer mass through the upper and lower boundaries of the cell. The flux through the upper boundary exactly equals the flux through the lower boundary of the cell above with opposite sign and the mass of the tracer is conserved in the column when using the Godunov scheme. The scheme used here is identical to the 1-D first-order version of the *Lin and Rood* [1996] transport scheme [*Lauritzen*, 2007]. The advantage of first-order finite-volume schemes is that they are inherently positive definite but they are usually considered too diffusive for long simulations. In this single-column model, however, the sources and sinks for the tracers are larger than the internal numerical diffusion; hence a low-order scheme can be justifiably used in this setting.

[15] Having predicted the change in tracer mass due to vertical transport, we convert it to mixing ratio by dividing the tracer mass $[X_i]\ \Delta p$ by Δp. Hereafter we update the mixing ratio due to horizontal divergence which obviously changes the total tracer mass in the column. It is noted that the discretization scheme used here preserves the mixing ratio for any prescribed ω field.

[16] Vertical velocities used to drive the model are (1) considered constant in time or (2) vary monthly. They are derived from European Center for Medium-range Weather Forecasts (ECMWF) analysis data for the years 2005 and 2006. Runs are with 2006 winds except where noted. Figure 2a illustrates tropical averaged vertical velocities for four seasons in 2006. The maximum tropical upwelling at all altitudes is found in December–February (DJF), and the minimum from the surface to 70 hPa in June–August (JJA). This seasonality is expected from the seasonality of the Brewer-Dobson circulation [*Rosenlof*, 1995].

[17] The ECMWF velocity field implicitly includes the impact of deep convection, which is treated separately in the model. Hence we also conduct sensitivity experiments in which the advective velocity is constrained to represent regions without deep convection. We do this using two methods. First, by selecting regions where the monthly mean outgoing longwave radiation (OLR) is greater than 240 W m^{-2}. This value was found to exclude broad regions of tropical deep convection over Africa, Indonesia, South America and the Intertropical Convergence Zone (ITCZ). OLR data were taken from National Oceanic and Atmospheric Administration (NOAA) interpolated OLR for the same time period as the ECMWF velocities (2006). NOAA interpolated OLR was obtained from the NOAA Earth System Research Laboratory, Physical Sciences Division (http://www.cdc.noaa.gov/). The second method sorts the vertical velocities for those regions where the cloud fraction (see below) is less than 0.15. This also eliminates the same regions, but also varies in altitude, providing a slightly finer screen. The thick gray lines in Figure 2a illustrate the effect of removing convective regions using these two methods (dark gray for cloud fraction, light gray for OLR): the clear sky advection in the troposphere changes sign and air is mostly subsiding ($\omega > 0$) up to the TTL. The effect on the model results is described in section 4.2.

[18] The model is coded in pressure coordinates, with Δp = 4 hPa. Vertical velocities are converted to pressure

coordinates (ω). The results are not strongly sensitive to the vertical coordinate (Δp = 2 hPa yields similar results).

3.2. Mixing

[19] Because the transport is explicitly mass conserving and strong convergence of vertical velocity exists in the TTL, we run some simulations with an optional mixing term to represent the other two dimensions of motions in the TTL. Mixing is parameterized as a relaxation to background conditions (zero source) with some characteristic time, so that

$$\frac{\partial [X_i]_{mix}}{\partial t} = -[X_i]\frac{(1-\Delta t/\tau_{mix})}{\partial t}, \quad (4)$$

where Δt is the time step in days and τ_{mix} is in days. In the standard runs, mixing is turned off.

3.3. Convection

[20] Convection is parameterized assuming a fractional source f and a source mixing ratio $[X_i]_{src}$ so that

$$\frac{\partial [X_i]_{conv}}{\partial t} = \alpha f \frac{([X_i]_{src}-[X_i])}{\partial t}. \quad (5)$$

Here α is a "convective efficiency" term that reflects how long it would take for 100% cloud cover to reset the mixing ratio to the surface source. Large-scale tropical convective systems have lifetimes of ~6 h (as measured by the autocorrelation of mean rain rates [see *Atlas et al.*, 1990]), and isolated lines of forced tropical thunderstorms may last 1–2 h [*Wilson and Megenhardt*, 1997]. We assume that the larger storms may efficiently detrain and mix tracers in the TTL (and have more than enough mass flux to do so), and that smaller storms may not completely replace all the air. So we set α = 1/3 h^{-1} (or a lifetime of 3 h). $[X_i]_{src}$ is chosen to be broadly representative of average tropospheric distributions of the four tracers. Thus $[X_i]_{src}$ equals 100 ppbv for CO, 600 pptv for C_2H_6, 50 ppbv for C_2H_2 and 1 pptv for ^{222}Rn. It is set to 1 pptv for CH_2Br_2, $CHBr_3$ and CH_3I.

[21] This formulation can be shown to be identical to an entraining and detraining mass flux convective scheme, for example, that of *Zhang and McFarlane* [1995] used in the NCAR Community Atmosphere Model [*Collins et al.*, 2006], if we neglect downdrafts and entrainment. The fractional source f is estimated using seasonal or monthly cloud fraction derived from the CloudSat 94-GHz cloud radar [*Stephens et al.*, 2008], shown in Figure 2b. CloudSat is a cloud radar that provides radar reflectivity from thick clouds; hence it is a good proxy for convection. Since tracer transport tends to follow the humidity transported in convection, f increases where the main convective outflow level (anvil clouds) is found.

3.4. Loss

[22] Loss of species is represented as a simple e-folding chemical lifetime τ_l where the time tendency of tracer $[X_i]$ at time t + 1 is based on the average value of $[X_i]$ (including convection and advection) over the time step; thus

$$\frac{\partial [X_i]_{loss}}{\partial t} = -[X_i]e^{(-dt/\tau_l)}. \quad (6)$$

[23] Chemical loss is a function of tracer lifetime. In this work we will focus on four representative tracers, CO, C_2H_6 (ethane), C_2H_2 (acetylene) and ^{222}Rn (radon), with τ_l in days of 60, 45, 15 and 4, respectively. We also examine CH_2Br_2 (dibromomethane), $CHBr_3$ (bromoform) and CH_3I (methyl iodide) with lifetimes of 120, 26 and 6 days, respectively.

[24] For CO, C_2H_6, C_2H_2 and CH_2Br_2, the atmospheric loss is due to oxidation by OH. For $CHBr_3$ and CH_3I, photolysis is the main loss [*World Meteorological Organization*, 2007]. In general, the lifetime is a function of OH and/or varies with solar flux and temperature. Here we have neglected these variations, which are likely not large in the TTL [*Sinnhuber and Folkins*, 2006]. For ^{222}Rn, radioactive decay is the main loss, and does not vary.

4. Results

[25] For steady state simulations, the model is run for 720 days with a time step of 1 h. The vertical domain is 0–40 km and Δp = 4 hPa. The vertical velocity (ω) at the top and bottom is set to zero; ω is constant in time for steady state runs. For examination of the annual cycle, it varies smoothly between monthly mean values (section 4.8). We will show results from the final time step for tendencies or tracer values. With constant advection, we can run the model to near equilibrium, that is $\frac{\partial [X_i]}{\partial t} = 0$. This is achieved for all but the longest-lived tracers (such as CH_2Br_2) after ~150 days. Final values are not sensitive to the initial conditions. Results of runs where the vertical velocity and convection are allowed to vary over time are shown in section 4.8 to investigate how the annual cycle affects the results and understand what drives the annual cycle.

4.1. Basic Results

[26] Results for the "base" case of the model with DJF tropical mean conditions are shown in Figure 3. Profiles from four tracers are shown: CO, C_2H_6, C_2H_2 and ^{222}Rn. The profiles have been normalized to their maximum value. Also shown is the scaled (by 0.5) cloud fraction (f).

[27] In general, the longer lifetime and lack of mixing allow tracers such as CO and C_2H_6 to build up to near emission levels in the troposphere. Some decay is seen in C_2H_2 and radon in Figure 3. Vertical advection causes the peak in tracer mixing ratio (seen clearly for radon in Figure 3) to be 1–2 km above the maximum convective outflow at 11 km. The mixing ratio peak is slightly higher for longer-lived species (but less distinct). Above this level, tracer concentrations tail off rapidly with height.

[28] Figure 4 illustrates the tracer concentrations in the TTL. In order to construct the values in Figure 4 and Table 2 for comparison to observations, annual means are used from the second year of runs with an annual cycle. Quantitatively, values are similar to an average of four seasonal steady state runs. Above 18 km, there is very little C_2H_2 or radon left, while for C_2H_6 (45-day lifetime) and CO (60-day lifetime) some tracer is lofted up to 20 km and higher. At 20 km, 3–5% of the "source" value remains for CO and C_2H_6 (Table 2).

[29] Simulated tracer values (Table 2 and Figure 4) quantitatively compare well to those from ACE (Table 1). ACE values at 20 km are slightly larger. This may be due to variations in vertical structure of loss, uncertainties in vertical

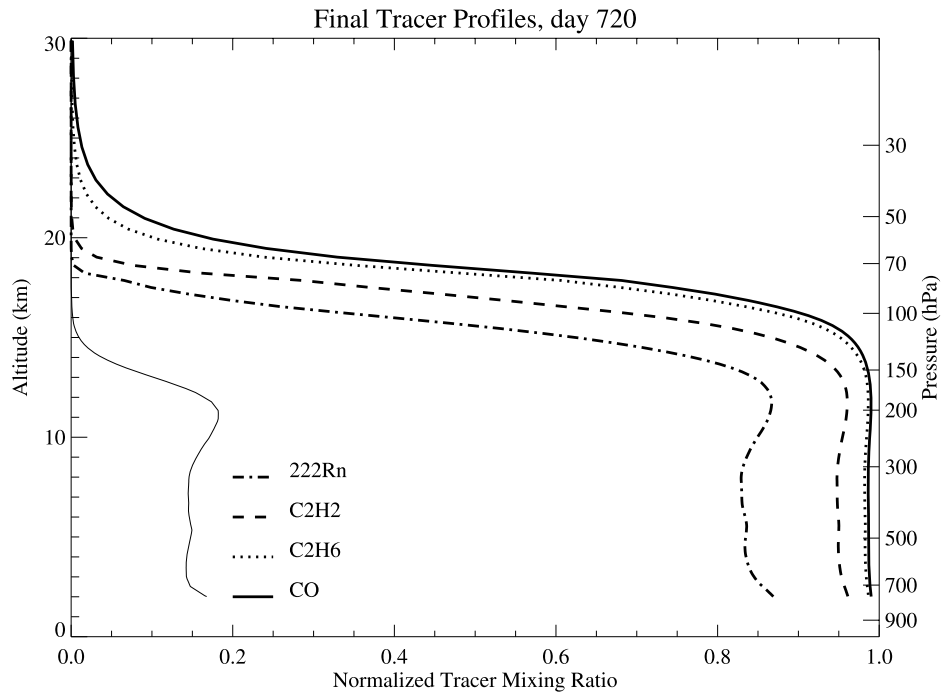

Figure 3. Final time normalized mixing ratios of CO (solid line), C_2H_6 (dotted line), C_2H_2 (dashed line), and radon (^{222}Rn: dash-dotted line) using DJF 2006 winds. Thin line is the cloud fraction profile (*f*) scaled by 0.5 for clarity.

velocity, or other sources. Observed CO does not go to zero in the stratosphere (Figure 1), so there is mixing and/or chemical sources, adding to the observed CO concentration (and not represented in the model). ACE fractions at 18 km just above the tropopause are similar to simulated values, while ACE fractions at 16 km are consistently smaller than the simulations, perhaps indicating different efficiency to convection as a function of height. This might be due to the fact that "overshooting" convection (convection above its level of neutral buoyancy) will tend to collapse rapidly back

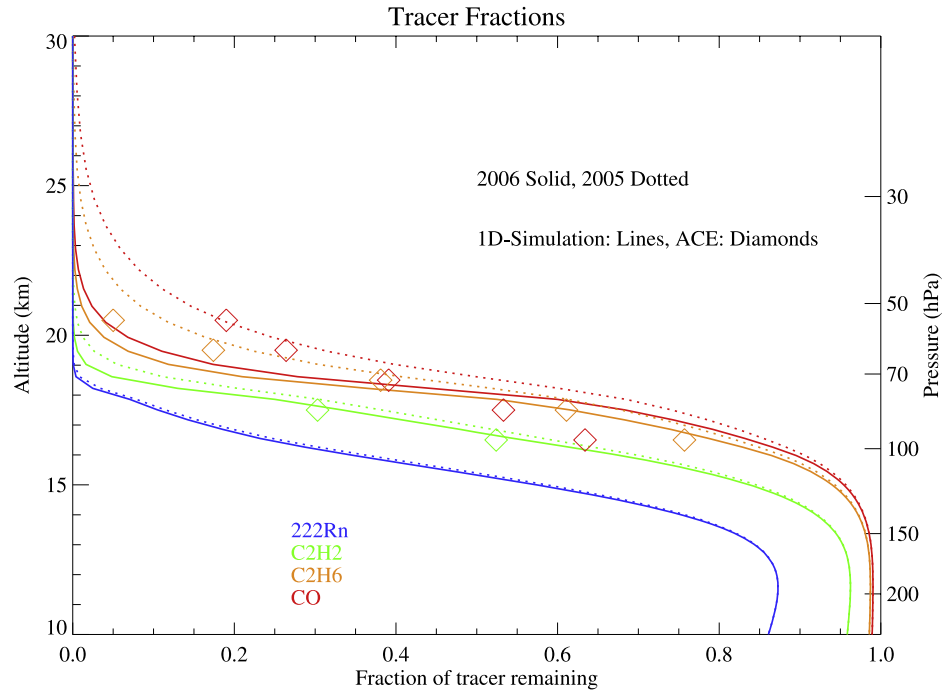

Figure 4. Annual mean normalized mixing ratios of CO (red), C_2H_6 (orange), C_2H_2 (green), and radon (^{222}Rn: blue) in the TTL. Solid lines represent runs with 2006 winds, and dotted lines are 2005 winds. ACE observations (normalized) shown as diamonds.

Table 2. Percent of Surface Source Remaining at Given Altitudes for Tracers With Different Lifetimes Based on Annual Averages of a Model Simulation With an Annual Cycle

Tracer	Lifetime, Days	Percent Remaining		
		16 km/100 hPa	18 km/79 hPa	20 km/58 hPa
CH_2Br_2	120	93	70	18
CO	60	87	52	5.3
C_2H_6	45	83	43	2.8
$CHBr_3$	26	74	28	0.6
C_2H_2	15	61	16	0.1
CH_3I	6	37	5.7	<0.1
^{222}Rn	4	28	3.6	<0.1

down and detrain at a lower level. But in general the model approach can reproduce the tracer decay observed from ACE. The convective efficiency (analogous to α in equation (5)), could be lowered or made a function of altitude to reflect "overshooting." This would better reproduce the observed tracer fractions from ACE in the upper troposphere. The efficiency would be reduced at higher altitudes above the level of neutral buoyancy (about 12–14 km). This has not been done in the simulations.

[30] The balance of terms in the model for each tracer is presented in Figure 5. Tendencies represent steady state values once the model has reached equilibrium ($\frac{\partial [X_i]}{\partial t} = 0$). For CO and C_2H_6, the convective source (CONV) dominates up to ~17 km, 2 km below the top of the convective region. The convective tendency is balanced by chemical loss (LOSS) and vertical advection (ADV). Advection is not important below the TTL (~200 hPa) where the convective source is large (see section 4.2 below). Vertical advection begins to dominate just above the cold point, with a spike as convection goes to zero. Advection is more important for longer-lived species. Small amounts of convection are able to maintain elevated mixing ratios several kilometers above the top of convection for longer-lived species.

4.2. Effect of Vertical Velocity

[31] As noted in section 3.1, vertical velocities from ECMWF include convective transport. This results in "double counting" the convective influence. We have tested this effect in several ways, but conceptually the most robust is to average the vertical velocity only over those regions without convection, as shown in Figure 2a (gray lines for DJF) using two methods. The vertical velocities now indicate subsidence $\omega > 0$ over a broad region of the troposphere, up to the TTL for both cases. Sorting by cloud fraction is done at each ECMWF level, so it is a finer grain sort than the column sort by OLR. Thus there is less subsidence, particularly above the convective peak.

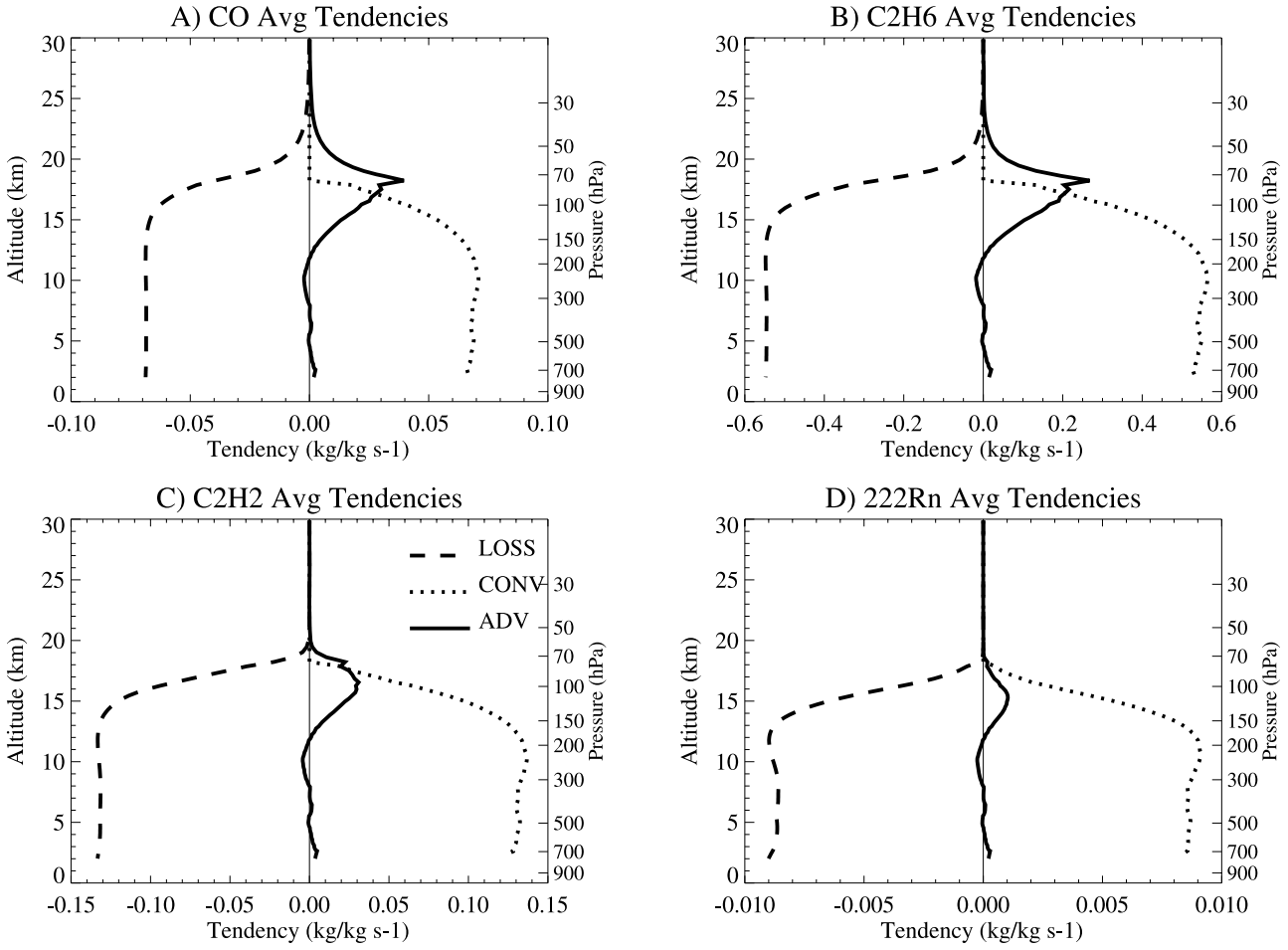

Figure 5. Final time tendencies of (a) CO, (b) C_2H_2, (c) C_2H_6, and (d) radon (^{222}Rn). Tendencies due to advection (ADV, solid lines); convection (CONV, dotted lines); and loss (LOSS, dashed lines).

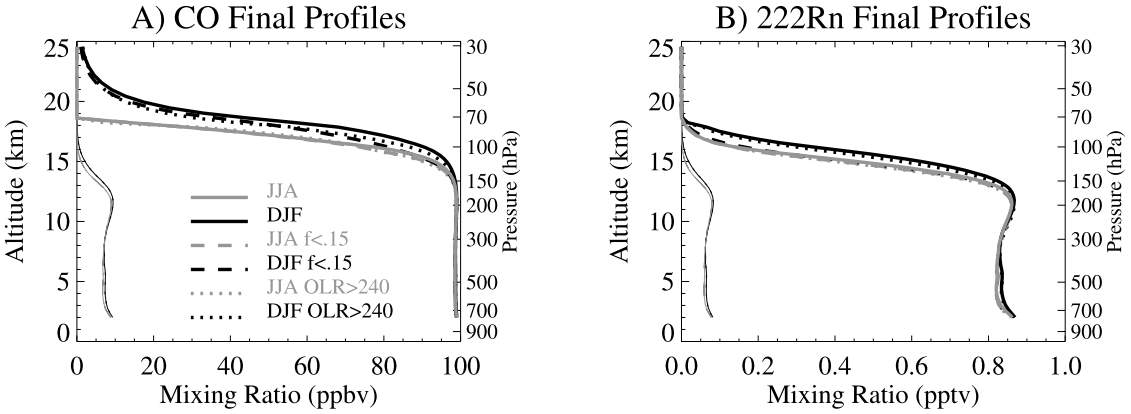

Figure 6. Final mixing ratio profiles of (a) CO and (b) radon (^{222}Rn) for DJF (black lines) and JJA (gray lines) for the standard case (solid lines), with vertical velocity (ω) averaged from regions where OLR > 240 W m^{-2} (dotted lines), and using ω sorted by cloud fraction where $f < 0.15$ (dashed lines). Cloud fraction (thin lines) scaled by 50 in Figure 6a and 0.5 in Figure 6b for clarity.

[32] The resulting model simulations with such ω profiles are shown in Figure 6 for CO and radon. Removing convective uplift has only a minor effect on the tracer mixing ratios. Quantitatively the fraction of tracer remaining at any altitude is 0–3% less for the sorted velocity (subsidence in the troposphere), lower for tracers with shorter lifetimes. This may seem surprising, but the result is logical because advection in the troposphere where subsidence occurs (below 100 hPa) is not an important part of the tracer tendencies and convection dominates (Figure 5). The effect of having subsidence in the troposphere slightly reduces the advective tendency from 150 to 100 hPa. If a sort by cloud fraction is used, there is little change in the balance of processes in the TTL. The annual cycle is not affected by a change in vertical velocity. Thus removal of convection from the vertical velocities does not qualitatively affect the model solutions. The quantitative effects are very small when the sort is done by cloud fraction, and preserves vertical velocities in the TTL above convective regions. This is because most of the difference in ω is below the level where advection dominates the tendencies.

[33] However, it is clear that above the peak in tracer mixing ratios and into the lower stratosphere, vertical velocities are critical for understanding tracer profiles. We explore this further by varying the vertical velocity profile in the simulations, again, for two tracers (Figures 7a and 7b for CO and radon), for two seasons (DJF and JJA). In Figure 7 we run six cases, with vertical velocity scaled by 0.25, 1 and 4 for DJF and JJA. Note that the downward velocity at 19–20 km in JJA (Figure 2a) is an effective cap on tracer propagation. For CO, the spread of tracer mixing ratios at 19–25 km in DJF is due to vertical velocity. For radon, this is still the case (higher vertical velocities have radon perhaps 1 km higher than the other cases). Changes below the convective peak at 12 km are small in both cases.

4.3. Sensitivity

[34] In this section we discuss the sensitivity of the model to various choices of parameters, including mixing and chemical loss.

4.3.1. Mixing

[35] Because the advection scheme in the model is strictly conservative for mixing ratio, we add an optional relaxation

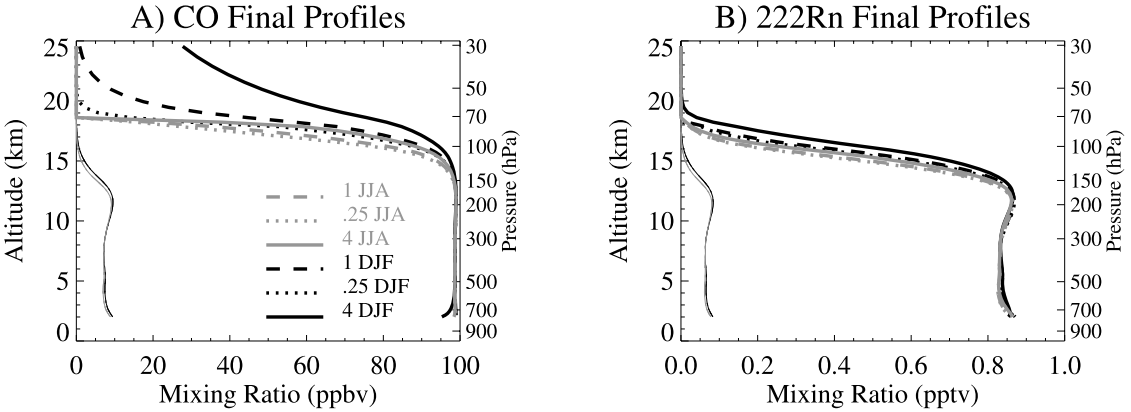

Figure 7. Final mixing ratio profiles of (a) CO and (b) radon (^{222}Rn) with different vertical velocities (ω scaled by 0.25, 1, and 4) for each of two seasons (DJF and June–August (JJA)). Cloud fraction (thin lines) scaled by 50 in Figure 7a and 0.5 in Figure 7b for clarity.

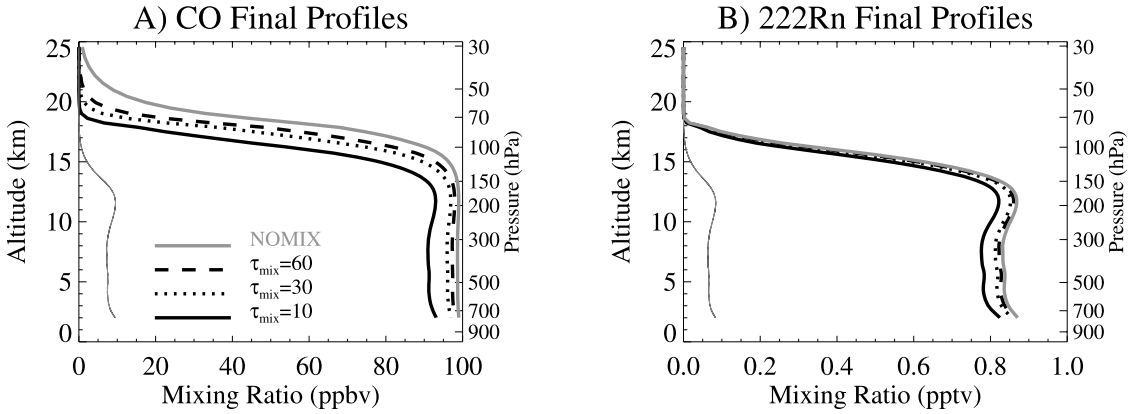

Figure 8. Final mixing ratio profiles of (a) CO and (b) radon (^{222}Rn) for different mixing assumptions using DJF 2006 winds. Mixing is set off (NOMIX) and with time scales of τ_{mix} = 10, 30, and 60 days. Cloud fraction (thin lines) scaled by 50 in Figure 8a and 0.5 in Figure 8b for clarity.

with a variable time scale. Shorter time scales imply stronger mixing. In the atmosphere, motion in the other two dimensions tends to effectively mix or diffuse a tracer. Thus we explore adding parameterized mixing to the model (equation (4)) to simulate these processes.

[36] Figure 8 illustrates the effect of adding a mixing term. Runs are performed with τ_{mix} = 60, 30, 10 (days) and no mixing, where longer times correspond to less mixing (equation (4)). Winds are from DJF 2006 and the model is run 720 days. Tracer concentrations throughout the column are reduced. For CO (Figure 8a), a longer-lived species, mixing dominates the total tracer tendency when it is less than the time scale for loss. For radon (Figure 8b), with a lifetime much shorter than mixing, loss still dominates since the mixing time scale is longer, and mixing does not affect the profile as much. Thus mixing is more important for longer-lived species.

4.3.2. Loss

[37] We have also explored several different alternative schemes for describing the chemical loss. These include changing the loss from an exponential decay to a linear ramp so that $\frac{\partial [X_i]}{\partial t} = [X_i] \frac{dt}{\tau}$. Then τ becomes the loss in percent per time step (or unit time). This change does not affect the solution appreciably. Changing the loss time scale by a factor of 4 does affect the profiles for short-lived species like radon, but is not as important for longer-lived tracers (such as CO). This is to be expected from the magnitude of tendency terms in Figure 5.

4.4. Seasonal Tests

[38] Figure 9 illustrates the impact of seasonal differences in convection and vertical motion on tracer profiles. Four runs are performed with winds from each season (DJF, MAM, JJA, SON) run for 720 days. In the tropical zonal average (±20° latitude) convective cloud fraction is nearly constant (Figure 2b), but does reach slightly higher altitudes in DJF. This impacts the tracer concentration up to 15 km. However, at 15 km and above, the largest effect is the difference in vertical velocity, which is higher throughout the TTL in DJF (Figure 2a). For the tropical average, it is the difference in vertical velocity that sets the seasonal cycle of tracer mixing ratios at the top of the TTL and in the stratosphere. This is also true for shorter-lived species (Figure 9b), but only below 18 km where significant tracer still exists. We return to this point after discussing the role of convection. Note that for JJA the average vertical velocity is nearly zero at ~19 km (Figure 2a), so tracer is

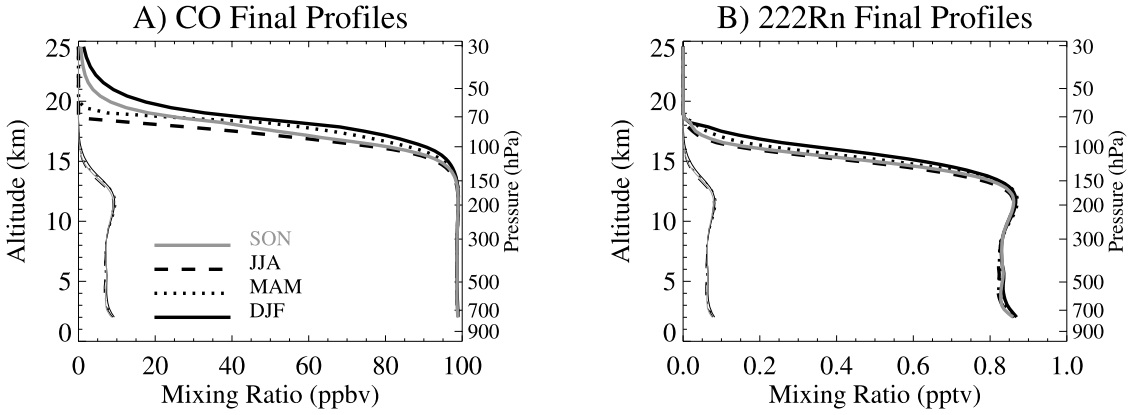

Figure 9. Final mixing ratio profiles of (a) CO and (b) radon (^{222}Rn) for DJF, March–May (MAM), JJA, and September–November (SON) using 2006 winds. Cloud fraction (thin lines) scaled by 50 in Figure 9a and 0.5 in Figure 9b for clarity.

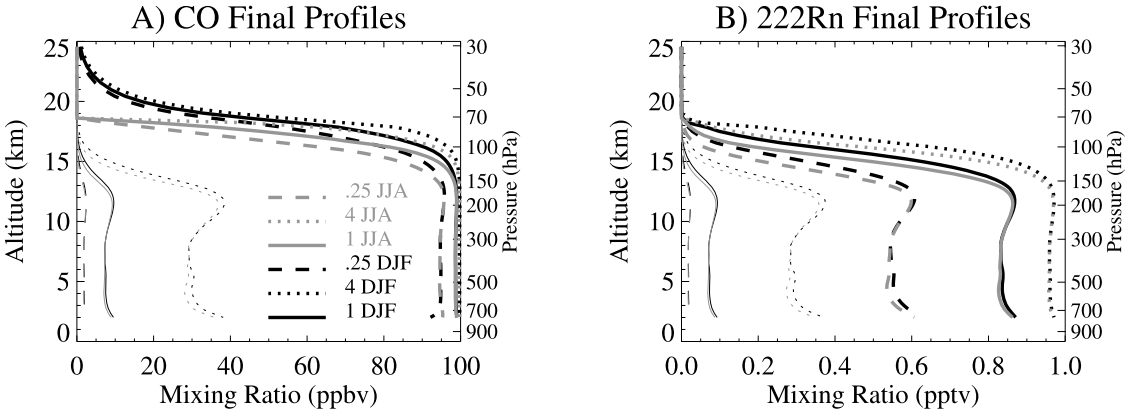

Figure 10. Final mixing ratio profiles of (a) CO and (b) radon (^{222}Rn) for convection with different magnitudes (*f* scaled by 0.25, 1, and 4) for each of two seasons (DJF and JJA). Cloud fraction (thin lines) scaled by 50 in Figure 10a and 0.5 in Figure 10b for clarity.

not advected above 19 km in a steady advection model in JJA.

4.5. Effects of Convection

[39] One of the main drivers of this work is to understand how a convective source of short-lived tracers effects the TTL. To examine this we vary convective strength, and discuss variations in the height of convection.

4.5.1. Convective Magnitude

[40] We have also varied the strength (magnitude) of convection, by scaling the convective source by a factor of 0.25, 1 and 4 in both DJF and JJA. The resulting simulations are shown in Figure 10. The thin lines show the different cloud fractions, (scaled by 0.5 for clarity on the plots) and the thick lines the resulting tracer profiles. Below the TTL, weaker convection leads to lower mixing ratios in both seasons, and stronger convection increases mixing ratios. For very strong convection, the profile is nearly locked to the convective source in both cases. Above the peak mixing ratio at 14–15 km however, the differences due to convection in Figure 10a for CO are small. Figure 10a indicates that differences in tracer mixing ratio above about 18 km are mostly seasonal: that is, they are due to differences in vertical velocity in the lower stratosphere, not due to convective input. For short-lived species such as radon, the strength of convection up to the top of convection does have an impact, but in no case does significant tracer end up in the stratosphere above 19 km. Thus the seasonal cycle of vertical velocity is more important than variations in convective magnitude above the tropopause.

4.5.2. Convective Top

[41] Because of the model construction, advection takes air and moves it from the convective region. If the vertical velocity is downward above the top of convection, this essentially "caps" the tracer transport. As indicated in Figure 2a, if the convective regions are removed from the velocity field, then there is an effective cap at 13 km (based on sorting by $f < 0.15$). Experiments indicate that allowing convection above this to 14 km will inject some tracer into the stratosphere, and allowing convection to 16 km or higher will allow a similar amount of tracer to reach the stratosphere as in a case with no cap on convection. Thus while it is important to sort out the true clear-sky vertical motion field in the TTL, it does not appear to affect tracer transport into the stratosphere as long as convection reaches at least 14–16 km. Note that there is clear sky radiative heating above 15 km [*Gettelman et al.*, 2004a] in the TTL. Motion between 12 and 15 km is complex, with subsidence and upward motion forced by the distributed wave effects of convection above the main convective outflow (see discussion by *Fueglistaler et al.* [2009]).

4.6. Regional Differences

[42] Finally, we decompose the vertical velocity from ECMWF analyses and CloudSat regionally and seasonally to look at variations in space as well as in time. We focus on four key regions and seasons: (1) the JJA Asian Monsoon (5°N–35°N, 60°E–120°E), the Western Pacific (20°S–20°N, 100°E–180°E) in (2) DJF and (3) JJA and (4) the Eastern Pacific (20°S–20°N, 180°E–270°E) in DJF. These regions are important for air entering the stratosphere (regions 1–3) or notable for being capped with upper level subsidence (region 4). Simulations using vertical velocities and convection for these four locations are illustrated in Figure 11 for CO and radon. Results based on the tropical average (MEAN) are also shown in Figure 11. In the regions with more convection than the tropical average (all but the Eastern Pacific), profiles are similar up to the peak at 13–15 km for both CO (Figure 11a) and radon (Figure 11b). The monsoon region in JJA has the highest CO (Figure 11a), but not the highest convection (found in the Western Pacific in DJF). Significant vertical motion associated with the monsoon anticyclone contributes to elevated tracer values. The Western Pacific in DJF has lower vertical velocities or even negative velocities around and above the cold point (noted first by *Sherwood* [2000] and *Gettelman et al.* [2000]). Thus convection and vertical velocity combine to create the TTL profiles of short-lived species. Convection is important in the troposphere and lower TTL, and vertical velocities dominate at the cold point and above.

4.7. Bromine and Iodine

[43] The model can be configured to represent different tracers with different chemical loss time scales. The set of tracers described above represents observed hydrocarbon

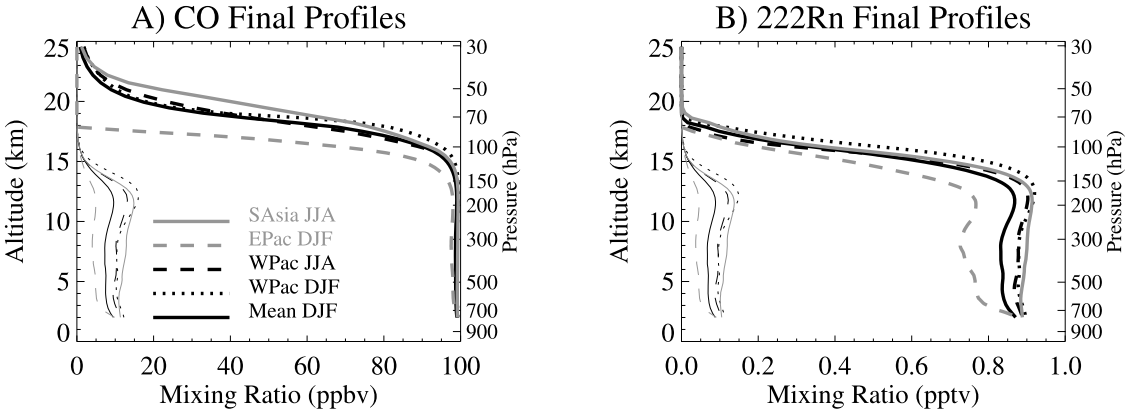

Figure 11. Final mixing ratio profiles of (a) CO and (b) radon (^{222}Rn) for different regions. SAsia (5°N–35°N, 60°E–120°E) in JJA, WPac (20°S–20°N, 100°E–180°E) in DJF, WPac in JJA, EPac (20°S–20°N, 180°E–270°E) in DJF, and the tropical mean. Cloud fraction (thin lines) scaled by 50 in Figure 11a and 0.5 in Figure 11b for clarity.

tracers with a range of lifetimes. We have also configured the model to represent tracers important for ozone concentrations in the stratosphere and stratospheric bromine and iodine. Figure 12 shows final concentrations in the TTL for a set of tracers with different lifetimes: CH_2Br_2 (120 days), $CHBr_3$ (26 days) and CH_3I (6 days). Figure 12 represents averages from a run with an annual cycle (similar to Figure 4). As expected, there is significant transport of CH_2Br_2, and not much transport of CH_3I above convection. $CHBr_3$ (bromoform) is an important reservoir of potential bromine for the stratosphere. Approximately 28% of the surface source makes it to 18 km in DJF as $CHBr_3$, while ~70% of CH_2Br_2 does (Table 2).

[44] Assuming boundary layer concentrations (and range) for CH_2Br_2 and $CHBr_3$ of 1.1 pptv (0.5–1.5) and 1.6 pptv (0.5–2.4) [*World Meteorological Organization*, 2007], this implies 0.8 pptv (0.35–1.1) CH_2Br_2 and 0.5 pptv (0.1–0.7) from $CHBr_3$. These values are within the range of $CHBr_3$ and CH_2Br_2 measurements reported by *Schauffler et al.* [1999], *Emmons et al.* [2000] and *Tuck et al.* [2004]. They are higher than results from [*Laube et al.*, 2008], but are well within the range of uncertainty given by variable boundary layer concentrations which may vary strongly from region to region. Assuming all this bromine would be released in the stratosphere, simulations imply that 2.8 pptv of bromine (range of 1.1–4.1 from observed

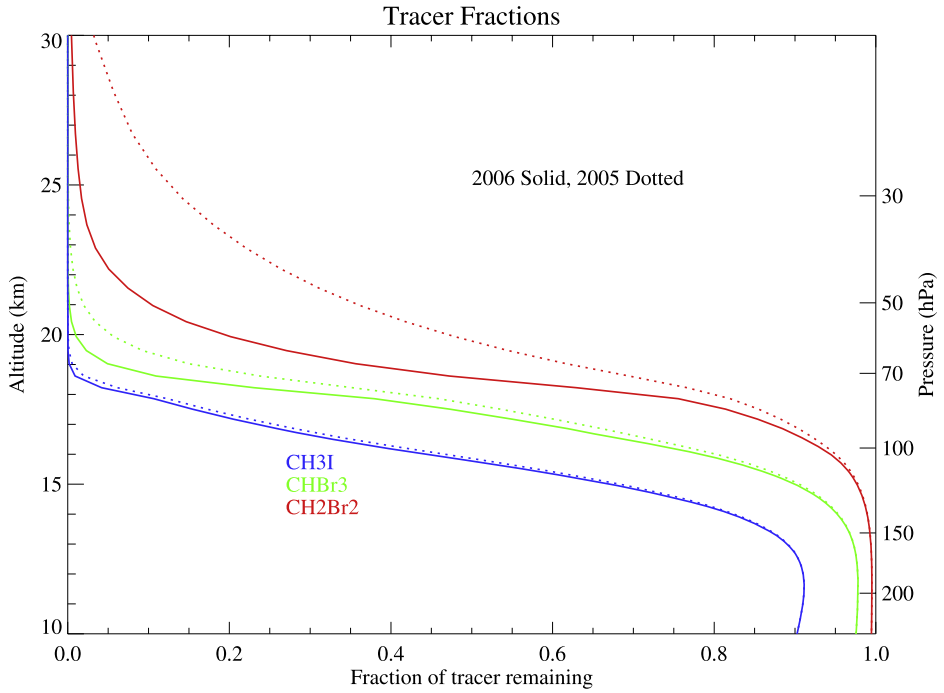

Figure 12. Average normalized mixing ratios of CH_2Br_2 (red), $CHBr_3$ (green), and CH_3I (blue). Solid lines represent runs with 2006 winds, and dotted lines are 2005 winds.

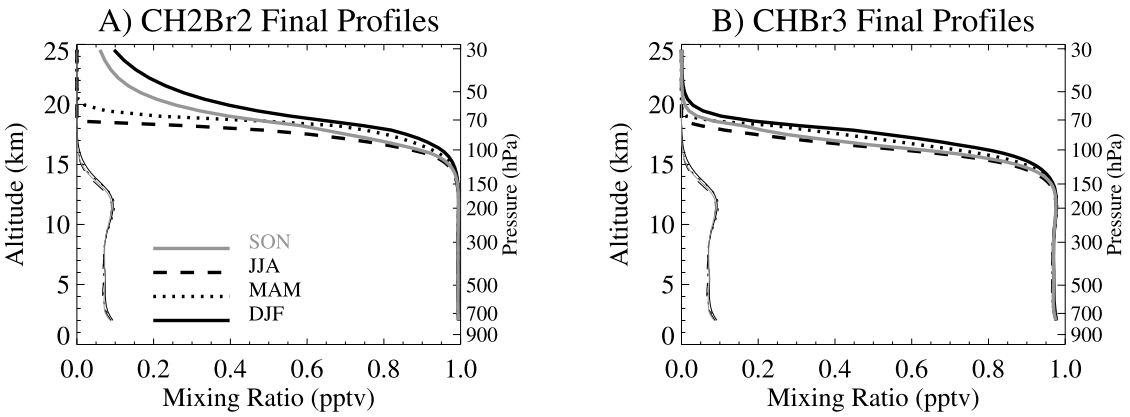

Figure 13. Final mixing ratio profiles of (a) CH_2Br_2 and (b) $CHBr_3$ for DJF, MAM, JJA, and SON. Cloud fraction (thin lines) scaled by 50 in Figure 13a and 0.5 for Figure 13b for clarity.

concentrations) may be entering the stratosphere as CH_2Br_2 and $CHBr_3$.

[45] As noted by *Sinnhuber and Folkins* [2006], the products of $CHBr_3$ oxidation can be rapidly removed by condensation onto ice, so lofting $CHBr_3$ above regions with cirrus clouds (above the cold point) is critical. The seasonal transport peaks in DJF with peak mean vertical velocities (Figure 13), consistent with Figure 9. Transport of $CHBr_3$ is more efficient in DJF owing to faster vertical velocities.

4.8. Annual Cycle

[46] The model can also be configured to run with time varying inputs of vertical velocity and/or convective sources. This allows exploration of the annual cycle of tracers in the TTL and lower stratosphere. For these simulations, the model was "spun up" for 120 days, and then run through a complete annual cycle using linear interpolation between monthly mean inputs (velocities and convection). Results can be compared to observations, and inputs can be held constant to understand which components (convection or vertical velocities) contribute to the annual cycle.

[47] Figure 14 illustrates concentrations (as a fraction of the source) for CO (Figure 14a) and C_2H_2 (Figure 14b). The BASE case at 70 hPa (solid lines) has a fairly large amplitude (0.1–0.55) with a peak in the early part of the year (February), just after the peak in vertical velocity, and a minimum in August (day 220), when velocities are negative in the lower stratosphere. The amplitude of the annual cycle is

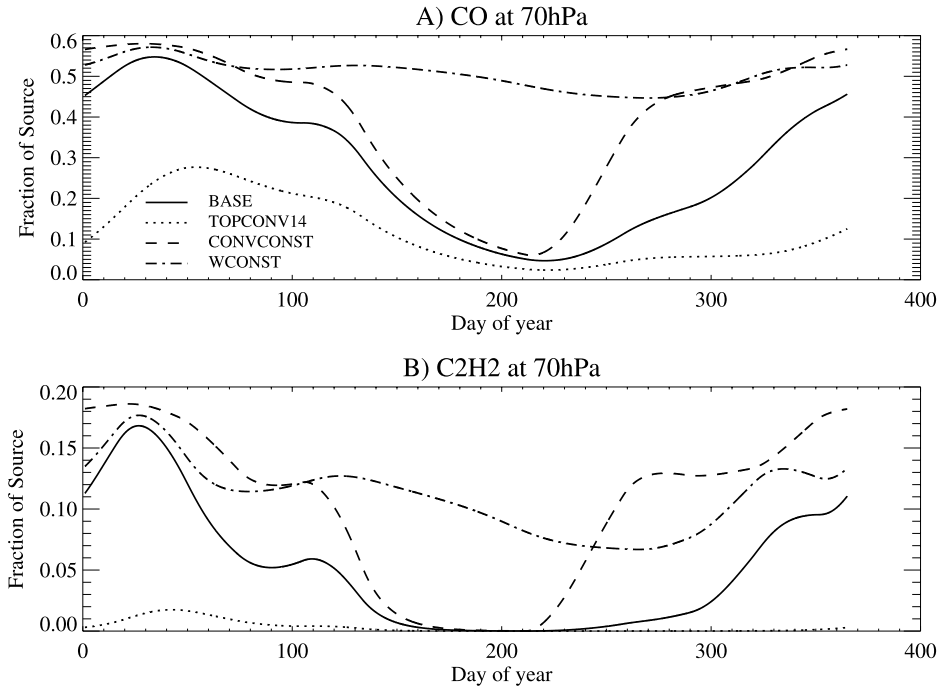

Figure 14. Normalized tracer mixing ratios as a function of time for (a) CO and (b) C_2H_2 at 70 hPa in a run with varying velocity and convection. Lines illustrate the BASE run (solid line), a run with convection only up to 14 km (TOPCONV14, dotted line), convection constant in time (CONVCONST, dashed line), and vertical velocities constant in time (WCONST, dash-dotted line).

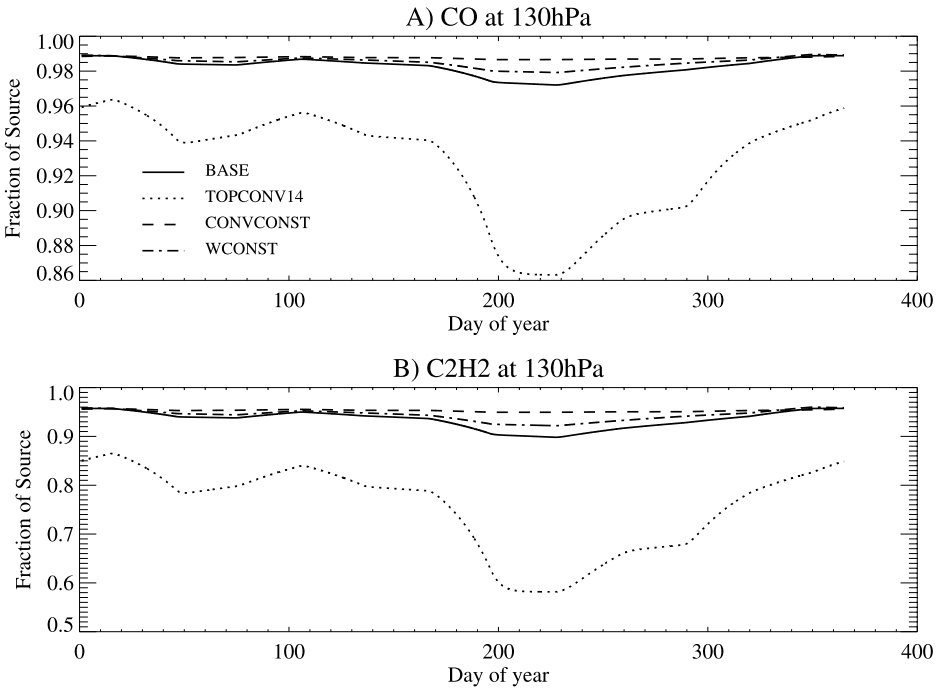

Figure 15. As for Figure 14 but for 130 hPa.

larger for C_2H_2 (almost no tracer remains in July–August), and the phase is similar (with extrema a few days earlier than CO). Also shown on Figure 14 are runs with convection limited to 14 km (TOPCONV14, dotted line), and with constant convection (CONVCONST, dashed line) or constant vertical velocity (WCONST, dash-dotted line).

[48] The capping of convection significantly reduces the tracer magnitude in Figure 14. It also slightly shifts the timing of the annual cycle, moving the maximum and minimum at 70 hPa for CO ~20 days later. The minimum in boreal summer also extends farther into fall. At 70 hPa, if convection is held constant over the year (CONVCONST) the annual cycle of mixing ratio changes slightly in September–December for CO or C_2H_2 (Figure 14, dashed line). However if vertical velocities are kept constant (WCONST), the annual cycle at 70 hPa is significantly reduced (Figure 14, dash-dotted line), consistent with steady state seasonal plots (Figures 9 and 13) illustrating the importance of variations in vertical velocity for stratospheric tracer concentrations [see also *Folkins et al.*, 2006; *Randel et al.*, 2007; *Schoeberl et al.*, 2008].

[49] The situation is slightly different at 130 hPa in the TTL below the tropopause (Figure 15). The annual cycle in the BASE case is very small for both tracers. The simulated amplitude of the tropical average annual cycle is less than observed. This may be partially expected since convective inputs move around spatially, but tropical averaged cloud fractions used in the simulations are nearly constant, and CO has defined source regions. Thus the model should not be expected to reproduce the total amplitude in the troposphere. The annual cycle amplitude increases (from 1% to 6% for CO) if rapid mixing (τ_{mix} = 10 days) is added (not shown). As in the lower stratosphere, capping the convective input at 14 km (TOPCONV14) lowers the tracer mixing ratio, and increases the relative amplitude of the annual cycle, but by a smaller amount (note the vertical scales are not the same in Figure 14 and Figure 15). Thus there is much less impact, particularly for CO, where the change in average tracer is from 98% to 92%. Note however that the annual cycle of convection and the vertical velocity now contribute significantly to the annual cycle, and most of the (small) annual cycle is supplied by variations in convection. Thus in any one region in the TTL below the tropopause, convection would be expected to impact the annual cycle of tracer distributions, even for tracers such as CO with lifetimes of 2 months.

[50] We can compare the seasonal cycle of CO to that observed from satellites, for example the Microwave Limb Sounder on the EOS Aura platform [*Schoeberl et al.*, 2006]. At 146 hPa, the observed seasonal cycle of CO is about 20 ppbv (or about 15% of the value at 146 hPa). In the model, there is almost no seasonal cycle. The tropospheric cycle is likely due to variations in emissions and convective mass fluxes. However, at 70 hPa, the seasonal cycle amplitude is about 12 ppbv, or 10% of the tropospheric source. The model has a large (40% of the tropospheric value) annual cycle at 70 hPa. The annual cycle is likely larger than observed owing to lack of a stratospheric background CO and mixing with such air. The timing of the CO seasonal cycle does agree with observations in the lower stratosphere. The minimum observed CO is from August to October, and the peak is in January. Thus the 1-D model is able to produce the seasonal cycle of CO in the lower stratosphere with no variation in emissions source, and also mostly with no variation in convection (Figure 14).

5. Conclusions

[51] This simple 1-D model allows some interesting insights into TTL transport.

[52] 1. The 1-D model can qualitatively and quantitatively reproduce the distribution of short-lived species in the TTL

using simple transport, convective source and parameterized loss. There are some differences in the slope of evanescent tracer mixing ratios between observations and simulations. The model is also able to generate the right phase of the annual cycle of CO, though it is quantitatively different than satellite observations in the upper troposphere and lower stratosphere owing to constant simulated emissions and simplified transport.

[53] 2. Convection is important up to the tropopause, and slightly above. There is little influence of velocities below the TTL (150–200 hPa) on the simulated tracer concentration in the lower stratosphere. Even for relatively long lived species like CO, a little convection contributes substantially to concentrations. However, large-scale vertical advection, though velocities are low, rapidly dominates above 15–17 km, though some convection goes up to 19 km.

[54] 3. The bifurcation point for significant transport into the stratosphere seems to be at a lifetime of 25–30 days, right around the lifetime of bromoform ($CHBr_3$). This is consistent with trajectory-based estimates of a TTL transit time of 60 days or so [*Fueglistaler et al.*, 2004] and a convective turnover time at 14 km of 2–3 months [*Gettelman et al.*, 2002b]. The fraction of tracer remaining at an altitude is a function of its lifetime. This is clearly seen in Figures 3 and 12, and quantitatively in Table 2.

[55] 4. Results allow further estimation of the transport of very short lived substances (VSLS) into the stratosphere. Seventy percent of the surface concentration of CH_2Br_2 is found at 18 km, while 52% of CO and 28% of $CHBr_3$ is. This implies that ~2.8 (1.1–4.1) pptv of additional bromine may be entering the stratosphere as CH_2Br_2 and $CHBr_3$, just over one half of the estimate of bromine from VSLS by *Dorf et al.* [2008].

[56] 5. Vertical velocity dominates tracer concentrations above the tropopause for tracers with lifetimes longer than a week (C_2H_2 and longer-lived species). This is clearly seen in both the steady state runs in different seasons, and in the runs over an annual cycle. Thus the seasonal cycle in CO above the tropopause in the lower stratosphere is due to the variation in vertical velocity in the lower stratosphere, not due to variations in the input concentration. With no variation in input concentration, the model is roughly able to produce the seasonality (phase) of CO in the lower stratosphere. This occurs even without variations in convective source, or in tropospheric emissions. Addition of a stratospheric background and a variable tropospheric emission (and loss) would improve agreement in the magnitude of the annual cycle in the upper troposphere. Vertical velocities below the TTL do not affect tracer concentrations in the TTL as long as some convection reaches a region in which clear sky velocities are upward (~15 km for radiative heating, possibly as low as 12 km for convective wave forcing).

[57] How would water vapor be placed in the context of this model? To the extent that water is a short-lived tracer in rapid vertical motion, convection should significantly impact the distribution of humidity, and it does. However, the process of condensation of water differs from chemical loss, as it is (1) reversible through evaporation and (2) strongly thermodynamically forced.

[58] While the simulations are in reasonable agreement with observations, there are still large uncertainties due to variability of short-lived tracer fields. The model could be developed further to fit observations by (1) adding a stratospheric source for CO and variable surface emissions ($[X_{CO}]_{src}$), (2) adjusting the convective efficiency (α) and (3) making chemical loss a function of altitude by relating it to OH concentrations and/or solar photolysis. Nonetheless, there are limitations of a 1-D model that limit the utility of further fitting to observations. For example, separating the vertical motion field into convective and nonconvective components for a complete diagnosis of vertical motion below the level of zero radiative heating at 15 km is a complex task. It is highly desirable to check these estimates and conclusions against further observations, and against full 3-D chemical transport models and/or coupled chemistry-climate models.

[59] **Acknowledgment.** The National Center for Atmospheric Research is sponsored by the United States National Science Foundation.

References

Atlas, D., D. Rosenfeld, and D. A. Short (1990), The estimation of convective rainfall by area integrals: 1. The theoretical and empirical basis, *J. Geophys. Res.*, *95*(D3), 2153–2160.

Bernath, P. F., et al. (2005), Atmospheric chemistry experiment (ACE): Mission overview, *Geophys. Res. Lett.*, *32*, L15S01, doi:10.1029/2005GL022386.

Collins, W. D., et al. (2006), The formulation and atmospheric simulation of the Community Atmosphere Model: CAM3, *J. Clim.*, *19*(11), 2122–2161.

Dorf, M., A. Butz, C. Camy-Peyret, M. P. Chipperfield, K. Kritten, and K. Pfeilsticker (2008), Bromine in the tropical troposphere and stratosphere as derived from balloon-borne BrO observations, *Atmos. Chem. Phys.*, *8*, 7265–7271.

Emmons, L. K., D. A. Hauglustaine, J. F. Müller, M. A. Carroll, G. P. Brasseur, D. Brunner, J. Staehlin, V. Thouret, and A. Marenco (2000), Data compositions of airborne observations of tropospheric ozone and its precursors, *J. Geophys. Res.*, *105*(D16), 20,497–20,536.

Folkins, I., and R. V. Martin (2005), The vertical structure of tropical convection and its impact on the budgets of water vapor and ozone, *J. Atmos. Sci.*, *62*, 1560–1573.

Folkins, I., P. Bernath, C. Boone, G. Lesins, N. Livesey, A. M. Thompson, K. Walker, and J. C. Witte (2006), Seasonal cycles of O_3, CO, and convective outflow at the tropical tropopause, *Geophys. Res. Lett.*, *33*, L16802, doi:10.1029/2006GL026602.

Fueglistaler, S., and P. H. Haynes (2005), Control of interannual and longer-term variability of stratospheric water vapor, *J. Geophys. Res.*, *110*, D24108, doi:10.1029/2005JD006019.

Fueglistaler, S., H. Wernli, and T. Peter (2004), Tropical troposphere-to-stratosphere transport inferred from trajectory calculations, *J. Geophys. Res.*, *109*, D03108, doi:10.1029/2003JD004069.

Fueglistaler, S., A. E. Dessler, T. J. Dunkerton, I. Folkins, Q. Fu, and P. W. Mote (2009), Tropical tropopause layer, *Rev. Geophys.*, *47*, RG1004, doi:10.1029/2008RG000267.

Gettelman, A., and T. Birner (2007), Insights on tropical tropopause layer processes using global models, *J. Geophys. Res.*, *112*, D23104, doi:10.1029/2007JD008945.

Gettelman, A., A. R. Douglass, and J. R. Holton (2000), Simulations of water vapor in the upper troposphere and lower stratosphere, *J. Geophys. Res.*, *105*(D7), 9003–9023.

Gettelman, A., W. J. Randel, F. Wu, and S. T. Massie (2002a), Transport of water vapor in the tropical tropopause layer, *Geophys. Res. Lett.*, *29*(1), 1009, doi:10.1029/2001GL013818.

Gettelman, A., M. L. Salby, and F. Sassi (2002b), The distribution and influence of convection in the tropical tropopause region, *J. Geophys. Res.*, *107*(D10), 4080, doi:10.1029/2001JD001048.

Gettelman, A., P. M. F. Forster, M. Fujuwara, Q. Fu, H. Vomel, L. K. Gohar, C. Johanson, and M. Ammeraman (2004a), The radiation balance of the tropical tropopause layer, *J. Geophys. Res.*, *109*, D07103, doi:10.1029/2003JD004190.

Gettelman, A., D. E. Kinnison, T. J. Dunkerton, and G. P. Brasseur (2004b), The impact of monsoon circulations on the upper troposphere and lower stratosphere, *J. Geophys. Res.*, *109*, D22101, doi:10.1029/2004JD004878.

Godunov, S. (1959), A difference scheme for numerical computation of discontinuous solutions of equations in fluid dynamics, *Math. Sb.*, *47*, 271.

Holton, J. R., and A. Gettelman (2001), Horizontal transport and dehydration in the stratosphere, *Geophys. Res. Lett.*, *28*(14), 2799–2802.

Laube, J. C., A. Engel, H. Bönish, T. Möbius, D. R. Worton, W. T. Sturges, K. Grunow, and U. Schmidt (2008), Contribution of very short-lived organic substances to stratospheric chlorine and bromine in the tropics—A case study, *Atmos. Chem. Phys.*, *8*, 7325–7334.

Lauritzen, P. H. (2007), A stability analysis of finite-volume advection schemes permitting long time steps, *Mon. Weather Rev.*, *135*(7), 2658–2673.

Lin, S. J., and R. B. Rood (1996), Multidimensional flux-form semi-Lagrangian transport schemes, *Mon. Weather Rev.*, *124*(9), 2046–2070.

Park, M., W. J. Randel, L. K. Emmons, P. F. Bernath, K. A. Walker, and C. D. Boone (2008), Chemical isolation of the Asian Monsoon anticyclone observed in atmospheric chemistry experiment (ACE-FTS) data, *Atmos. Chem. Phys.*, *8*, 757–764.

Randel, W. J., M. Park, F. Wu, and N. Livesey (2007), A large annual cycle in ozone above the tropical tropopause linked to the Brewer-Dobson circulation, *J. Atmos. Sci.*, *64*, 4479–4488.

Read, W. G., D. L. Wu, J. W. Waters, and H. C. Pumphrey (2004), Dehydration in the tropical tropopause layer: Implications from the UARS Microwave Limb Sounder, *J. Geophys. Res.*, *109*, D06110, doi:10.1029/2003JD004056.

Read, W. G., M. J. Schwartz, A. Lambert, H. Su, N. J. Livesey, W. H. Daffer, and C. D. Boone (2008), The roles of convection, extratropical mixing, and in-situ freeze-drying in the tropical tropopause layer, *Atmos. Chem. Phys.*, *8*, 6051–6067.

Rosenlof, K. H. (1995), Seasonal cycle of the residual mean meridional circulation in the stratosphere, *J. Geophys. Res.*, *100*(D3), 5173–5191.

Salawitch, R. J., D. K. Weisenstein, L. J. Kovalenko, C. E. Sioris, P. O. Wennberg, K. Chance, M. K. W. Ko, and C. A. McLinden (2005), Sensitivity of ozone to bromine in the lower stratosphere, *Geophys. Res. Lett.*, *32*, L05811, doi:10.1029/2004GL021504.

Schauffler, S., E. Atlas, D. Blake, F. Flocke, R. Lueb, J. Lee-Taylor, V. Stroud, and W. Travnicek (1999), Distributions of brominated organic compounds in the troposphere and lower stratosphere, *J. Geophys. Res.*, *104*(D17), 21,513–21,535.

Schoeberl, M. R., B. N. Duncan, A. R. Douglass, J. Waters, N. Livesey, W. Read, and M. Filipiak (2006), The carbon monoxide tape recorder, *Geophys. Res. Lett.*, *33*, L12811, doi:10.1029/2006GL026178.

Schoeberl, M. R., et al. (2008), QBO and annual cycle variations in tropical lower stratosphere trace gases from HALOE and aura MLS observations, *J. Geophys. Res.*, *113*, D05301, doi:10.1029/2007JD008678.

Sherwood, S. C. (2000), A stratospheric "drain" over the maritime continent, *Geophys. Res. Lett.*, *27*(5), 677–680.

Sherwood, S. C., and A. E. Dessler (2001), A model for transport across the tropical tropopause, *J. Atmos. Sci.*, *58*, 765–779.

Sinnhuber, B. M., and I. Folkins (2006), Estimating the contribution of bromoform to stratospheric bromine and its relation to dehydration in the tropical tropopause layer, *Atmos. Chem. Phys.*, *6*, 4755–4761.

Stephens, G. L., et al. (2008), Cloudsat mission: Performance and early science after the first year of operation, *J. Geophys. Res.*, *113*, D00A18, doi:10.1029/2008JD009982.

Tuck, A. F., et al. (2004), Horizontal variability 1–2 km below the tropical tropopause, *J. Geophys. Res.*, *109*, D05310, doi:10.1029/2003JD003942.

Wilson, J. W., and D. L. Megenhardt (1997), Thunderstorm initiation, organization and lifetime associated with Florida boundary layer convergence lines, *Mon. Weather Rev.*, *125*(7), 1507–1525.

World Meteorological Organization (2007), Scientific assessment of ozone depletion: 2006, *WMO Rep. 50*, Geneva, Switzerland.

Zhang, G. J., and N. A. McFarlane (1995), Sensitivity of climate simulations to the parameterization of cumulus convection in the Canadian Climate Center general circulation model, *Atmos. Ocean*, *33*, 407–446.

A. Gettelman and M. Park, Atmospheric Chemistry Division, National Center for Atmospheric Research, Boulder, CO 80305, USA. (andrew@ucar.edu)

J. E. Kay and P. H. Lauritzen, Climate and Global Dynamics Division, National Center for Atmospheric Research, Boulder, CO 80305, USA.